WARWICK
THE UNIVERSITY OF WARWICK

Executive Summary of PhD Thesis

The first fleet of nuclear power plants commissioned in the UK for commercial power generation were the Magnox type nuclear reactors and were named after the Magnox fuel elements used within the reactor. In total, 26 Magnox nuclear power plants were constructed within the UK and after many decades of operation, all of these nuclear power plants have now reached the end of their useful life cycle and are now in the process of being decommissioned (1; 2; 3; 4; 5; 6). Under the guidance of the Nuclear Decommissioning Authority (NDA), a public body of the UK government that delivers the decommissioning and clean-up of the UK's legacy nuclear assets in a safe, secure, and cost-effective way, all Magnox reactors have been defueled. The spent fuel is consolidated at the fuel handling plant at the Sellafield site for reprocessing, where the fuel is separated into different product streams. One product of the reprocessing of spent nuclear fuel is plutonium dioxide (PuO_2) and is packaged into a type of special nuclear material (SNM) containment known as Magnox packages. A Magnox package is constructed from three parts: an aluminium inner container which stores the PuO_2, a polyethylene intermediate container and an outer 316L stainless steel container which is sealed with a resistance seam weld between the container body and the container lid. Figure 1 shows an image of the inner and outer container of a Magnox package. In line with government policy, the Magnox packages are stored within specialist facilities until a long-term solution is implemented (7).

Figure 1: A photograph of the inner container of a Magnox package on the left, and the outer container on the right. (2)

Elizabeth Sharp

Within the inner containment of the Magnox package, intricate radiation chemistry mechanisms take place as the package resides within storage facilities, posing a novel challenge for the nuclear industry. The production of hydrogen and helium gas, from radiolysis and the alpha decay of plutonium-241 and americium-241, respectively, causes the air gap between the intermediate and outer container of the package to become pressurised. Additional reactions also contribute to the internal pressurisation of the Magnox package. For example, the inner containment atmosphere contains a 50:50 air/argon mix and is prone to pressurisation as a result of the increased internal package temperature, furthermore hydrogen gas is also produced from the decomposition of water (4) (8) (9). The potential for elevated internal pressures within the packages has heightened concerns regarding package integrity and the safe, secure, and long-term storage of these containers. The complexity of the industrial problem grows, as previous studies have shown that some of the surface reactions of plutonium dioxide, such as radiolysis, are both reversible and irreversible. This can lead to fluctuations in the pressurisation of the package, such that packages can pressurise and also depressurise over time. Optical inspection techniques are deployed within the storage facilities to oversee the packages, and analysis of the camera's video output across various inspection periods has detected visible degradation in certain packages. This degradation manifests as bulging on both the base and lid of the outer package. Furthermore, laser measurements have been conducted to gauge alterations in package length, which are then used to estimate internal pressure levels. Both techniques are subject to multiple limitations. For instance, the video output provides only a qualitative assessment of the package, while laser measurements rely on a linear relationship between package deformation and internal pressure. This assumption disregards the potential for reversible reactions of the plutonium dioxide, which could lead to both pressurisation and depressurisation. Moreover, legacy containment stores lack support for any form of inspection procedure, exacerbating the challenge. The inability to perform quantitative measurements of package pressure, the inaccuracy of current inspection methods, and the absence of inspection capabilities in legacy stores collectively underscore the imperative for developing a suitable inspection technique capable of accurately measuring Magnox package internal pressure.

In the thesis presented, vibrational resonance testing serves as the principal measurement technique to assess alterations in the vibrational response of the Magnox

package, when subjected to increased and decreased internal pressures and reduced material rigidity due to temperature increases. The practice of measuring an object's vibrational response has been a staple in diagnostic testing for decades, tracing its origins back to the wheel-tap test. This method entails applying force to an object for analysis of its audible acoustic response. Any deviation from a previously recorded response of a defect-free object signals potential structural issues. An object's vibrational response is unique, defined by a distinct set of characteristic vibrational resonant frequencies—a diagnostic fingerprint determined by physical parameters such as mass, elasticity, and boundary conditions. Hence, modifications to these parameters result in corresponding changes in the object's vibrational behaviour. Therefore, any changes to one of these parameters is reflected in a change in the object's vibrational response. While there exist various methods for measuring the vibrational response of an object, the chosen measurement technique needed to align with specific criteria outlined by the industrial partner. These criteria stipulated that the technique must be non-contact, non-destructive, and acoustic in nature. An approach that fulfils these requirements is the use of electromagnetic acoustic transducers (EMATs).

EMATs are a type of non-contact transducer that utilise electromagnetic transduction mechanisms to generate and detect acoustic and ultrasonic waves within a conducting material, without requiring any contact with the surface of the sample. In the context of the presented thesis, EMATs have been used to excite the vibrational resonant frequencies and subsequently detect the change in these vibrational resonant frequencies of the Magnox package over a range of internal pressures. The configuration of a typical EMAT transducer requires a wire wrapped around or in the proximity of either a permanent or electromagnet. A varying current is passed through the wire, generating a time-varying magnetic field within the sample's surface to a depth that is characterised by the electromagnetic skin depth. This induces and electric field on the sample's surface, causing free conducting electrons within the sample to experience a Lorentz force. The resultant kinetic energy of the free electrons is completely transferred to the ions of the metallic crystal lattice causing coherent motion of the ions, thus generating an elastic wave in the material. For simplification of this thesis summary, the reception of acoustic and ultrasonic waves by an EMAT detector follows the reverse process of the generation mechanism. A "self-field" generator EMAT, utilising solely the dynamic magnetic fields generated from the coil, was meticulously designed, and constructed to induce vibrational frequencies within the Magnox outer container wall. The EMAT's configuration ensured

that the dynamic magnetic fields ran parallel to the material surface, generating forces perpendicular to the sample surface. This design facilitated the propagation of lamb-like radial acoustic and ultrasonic waves within the wall material. The generation of acoustic and ultrasonic waves within the material was further augmented by incorporating a ferrite back-plate behind the EMAT coil, thereby significantly amplifying the eddy currents and Lorentz forces within the package wall. The detector EMAT featured a linear coil wound around a central magnet stack comprising three magnets, which supplied a tangential static magnetic field into the container wall. This setup enabled the EMAT to measure the out-of-plane vibrations of the container wall. Electromagnetic simulation models confirmed that the stacked magnet arrangement enhanced the magnetic flux density and linear magnetic field within the material wall. Experimental measurements corroborated these findings, demonstrating a discernible increase in peak-to-peak voltage when measuring the out-of-plane vibrations. Notably, Figure 2 below displays photographs of the bottom faces of the generator EMAT (Left) and the detector EMAT (Right).

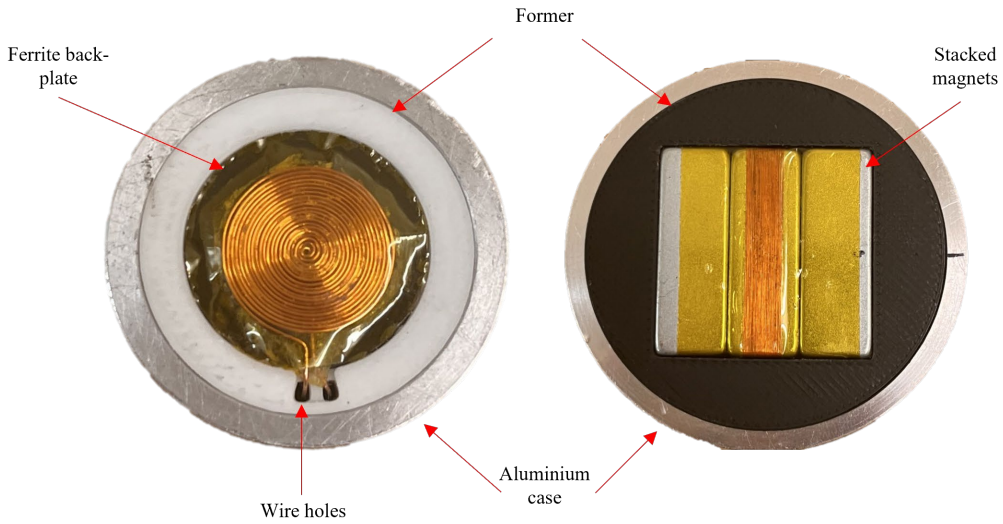

Figure 2: (Left) A photo of the bottom face of the generator EMAT. (Right) A photo of the bottom face of the detector EMAT.

Initially the vibrational resonant frequencies and corresponding mode shapes of a Magnox package were simulated using a finite element (FE) model. A cylindrically symmetric FE model of the Magnox package was constructed in SolidWorks, with certain assumptions applied to streamline model complexity and solve time, all while preserving model integrity. The FE model estimated a spectrum of 250 eigenfrequencies and eigenmodes, generating various mode shape patterns across the Magnox package wall. An

experimental setup was devised to induce vibrations in the Magnox package using the generator EMAT, which provided a broad-spectrum excitation to the package wall, spanning frequencies up to 200 kHz, with the primary excitation frequency centered around 20 kHz. To measure the out-of-plane velocity of the Magnox containment wall across a range of angular and length positions, a Laser Doppler Vibrometer (LDV) was employed. This facilitated the generation of mode shape profiles for numerous vibrational resonant frequencies, which were subsequently compared with the FE model outputs.

The vibrational resonant frequencies of the Magnox package were investigated by firstly converting each point from a velocity-time measurement to a displacement-time measurement. Subsequently, a Fast Fourier Transform (FFT) was applied to ascertain the spectral response of the package. The peak frequency data extracted from the FFT facilitated the design of a bandpass filter, tailored to the specific vibrational resonant frequency of interest. This filter was then employed to refine the displacement measurements of the package wall, allowing for focused analysis around the targeted resonant frequency. To visually compare the FE model estimated eigenmodes with the experimentally measured mode shapes of the package wall, corresponding mode shape displacement profiles for similar vibrational frequencies were plotted in the form of an image plot, as shown in Figure 3.

The first column of image plots in Figure 3 depicts the experimentally measured displacement profiles for the frequencies 708 Hz, 984 Hz, and 1189 Hz. In the second column of image plots in Figure 3, the estimated FE displacement profiles for the frequencies 724 Hz, 1005 Hz, and 1186 Hz are presented. To compare the experimental and FE model displacement profile data, a signal analysis method was devised and employed. Initially, the experimental and FE displacement data for a specific vibrational resonant frequency were evaluated across the same angular and length range.

Subsequently, the experimentally measured and FE modelled displacements of the package wall were examined for a series of vibrational modes at a predetermined height of the package wall. A sine function was then fitted to both the experimental and FE displacement data, utilising a least squares fitting approach, and the wavelength coefficients from the fits were extracted and compared. The comparison between the experimental results and the FE model results has demonstrated favourable agreement between the two datasets.

The first column of image plots in figure 3 are the experimentally measured displacement profiles for the frequencies 708 Hz, 984 Hz and 1189 Hz. In the second column of image plots in figure 3 are the estimated FE displacement profiles for the frequencies 724 Hz, 1005 Hz and 1186 Hz. A signal analysis method was created and used to compare the experimental and the FE model displacement profile data. Firstly, the experimental displacement data and the FE displacement data for a particular vibrational resonant frequency were evaluated over the same angular and length range. The experimentally measured and the FE modelled displacements of the package wall were then inspected for a series of vibrational modes at a set height of the package wall. A sine function was then fitted to both the experimental and FE displacement data, using a least squares fitting approach and the wavelength coefficient from the fits were extracted and compared. The comparison between the experimental results and the FE model results have shown good agreement between the measured vibrational resonant frequencies with the compared FE model eigenfrequencies. Numerous calculated wavelengths derived from the displacement of the package wall closely align with or fall within the error margins of each wavelength value. This similarity observed among the mode shape displacement profiles, the vibrational resonant frequencies, and the calculated wavelengths of both the experimental data and the FE data suggests that the FE model is adept at modelling various vibrational resonant frequencies of the Magnox package. Nonetheless, it is prudent to anticipate some discrepancies between the experimental results and the FE model results, given that the model serves as an approximation of the Magnox package.

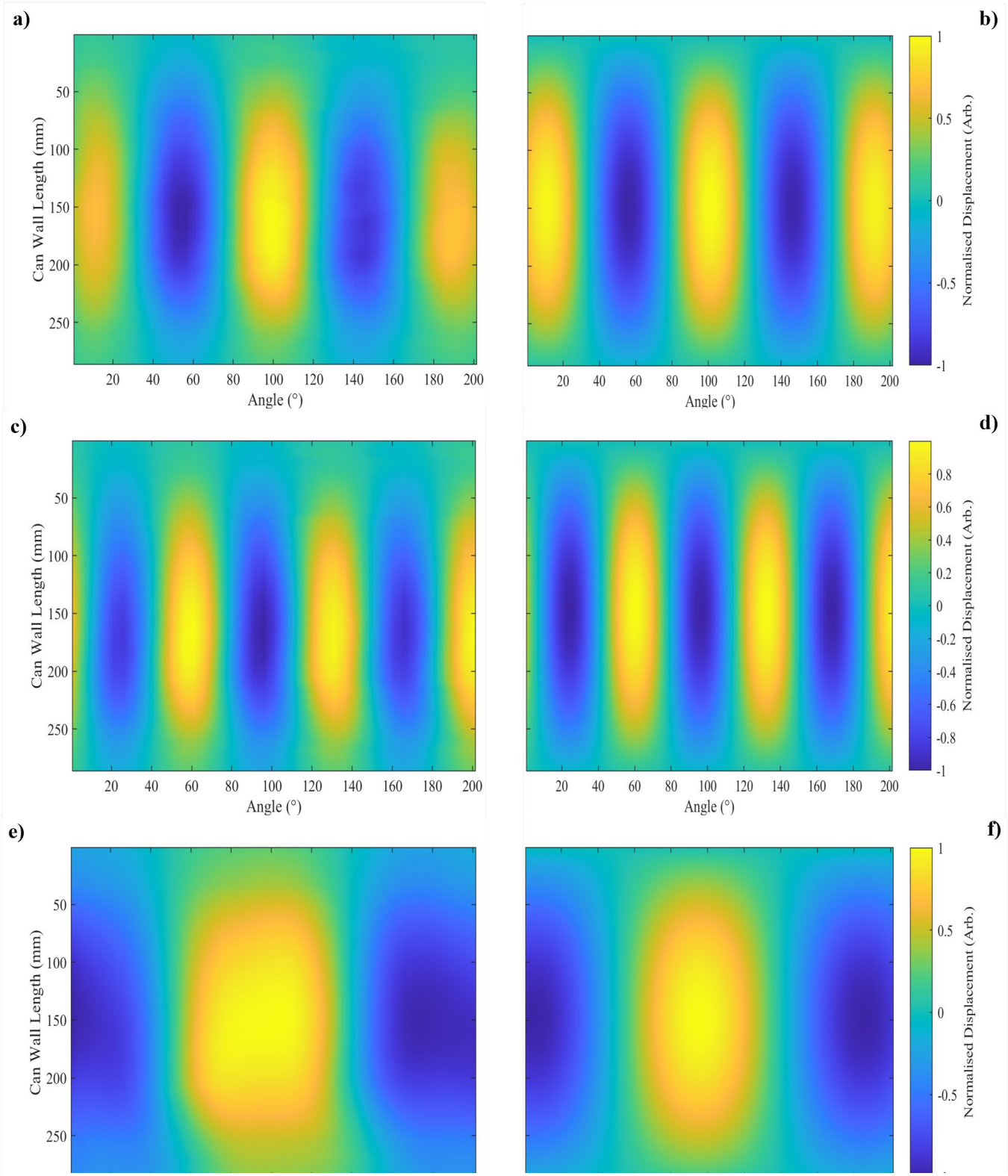

Figure 3: The image plots a), c) and e) show the mode shape displacement profile that has been experimentally measured and smoothed using a moving mean, for the vibrational resonant frequencies, 708 Hz, 984 Hz and 1189 Hz. The image plots b), d) and f) are the corresponding FE model predicted mode shape displacement profiles for the vibrational resonant frequencies of 724 Hz, 1005 Hz and 1189 Hz.

During the PhD phase, the primary focus was to explore the impacts of escalating internal pressure on the Magnox package. Subsequently, during my postdoctoral research, measurements pertaining to depressurisation were acquired, providing valuable insights into the behaviour of the package under varying pressure conditions.

The investigation into the change in vibrational resonant frequencies resulting from increasing internal pressure of the Magnox package was conducted both experimentally and computationally, utilizing the same FE model previously mentioned. The FE model underwent adaptation to facilitate the application of pressure loads to the Magnox package walls, enabling the calculation of eigenfrequencies across a range of internal pressures, from atmospheric pressure to 3 bar, in 0.2 bar intervals. Experimental measurements were conducted on the Magnox package over the same pressure range and interval used in the FE model. The generator EMAT was positioned at the midpoint of the package wall to induce vibrations, while the detection EMAT and pressure field microphone, placed with a 180° circumferential separation from the generator EMAT, measured the out-of-plane displacement fields and generated pressure fields, respectively, as amplitude-time signals at each pressure interval.

A pressure field microphone served as a comparative detection method against the EMAT detector, given that reception of certain vibrational frequencies may be slightly diminished when the detection EMAT is situated at a node position of the mode shape on the package wall. The eigenfrequencies were extracted from the FE model, and an FFT was applied to the amplitude-time signals measured by the detection EMAT and the pressure field microphone at each pressure interval to extract the spectral response of the package. The peak frequency shift of the experimentally measured vibrational frequencies and the FE model estimated eigenfrequencies were plotted against the internal pressure of the Magnox package, as depicted in Figure 4. The graphs presented in Figure 4 illustrate that as the internal pressure of the package increases, both the experimentally measured vibrational frequencies and the model-estimated eigenfrequencies exhibit an increase in peak frequency value. However, the rate at which the vibrational frequencies increase in peak frequency value varies among each vibrational frequency. Variations between the model and the experimentally measured vibrational resonant frequencies are to be expected, given that the model approximates the Magnox package's behaviour.

To inspect the behaviour of the vibrational resonant frequencies of the Magnox package across a range of internal pressures, an image plot for the EMAT-detected measurements was generated. In Figure 5, the image plot comprises each FFT output of

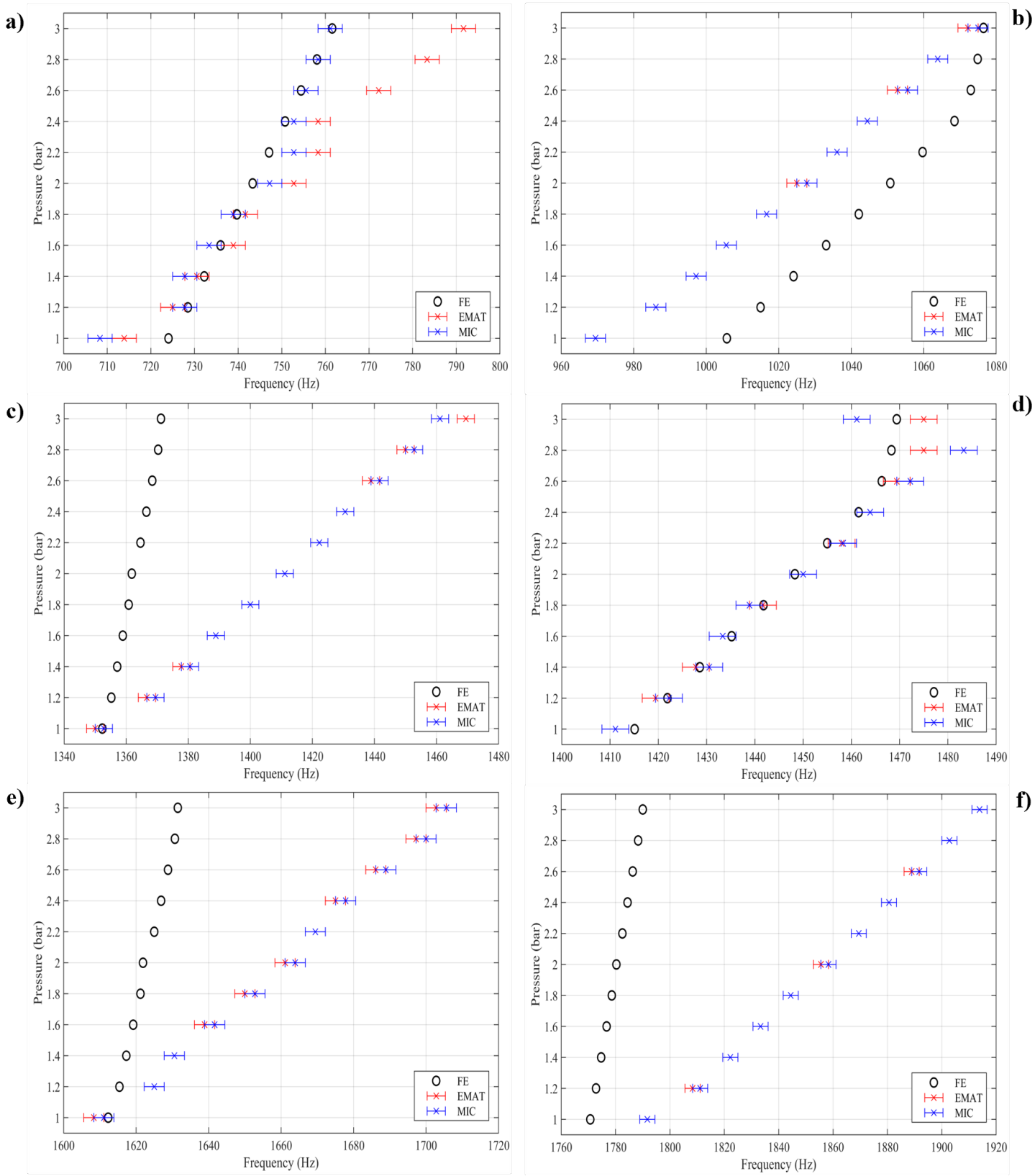

Figure 4: The plots a) to f) present the peak frequency shifts of 6 different vibrational resonant frequencies measured by the EMAT detector and the pressure field microphone, and the corresponding FE model predicted eigenfrequency shifts from atmospheric pressure to 3 bar.

of the amplitude-time signals recorded at pressure intervals ranging from atmospheric pressure to 3 bar. The x-axis of the image plot represents the frequency of the spectra in kilohertz, while the y-axis depicts the range of pressures. A normalized magnitude colour bar is utilised to portray the magnitude of the vibrational resonant frequencies of the Magnox package wall. Within the spectra, the large magnitude peaks, depicted by the light blue to yellow colour region of the colour bar, surpass the noise level and signify the vibrational resonant modes of the package wall. Conversely, the low magnitude peaks of the spectra are presented by the dark blue colour region of the colour bar. Notably, the vibrational resonant frequencies measured at atmospheric pressure, characterised by the large magnitude peaks within the spectra, demonstrate an increase in peak frequency value and a shift towards the right of the spectra with increasing internal pressure of the Magnox package. This trend is expected and is evident across the entire frequency range of 0 kHz to 5 kHz. As the internal pressure of the Magnox package increases, the structural stiffness of the package correspondingly increases. This increase in stiffness is mirrored by a change in the elastic response of the package wall, where the measured vibrational resonant frequencies exhibit an increase in frequency value as the pressure within the package rises (13).

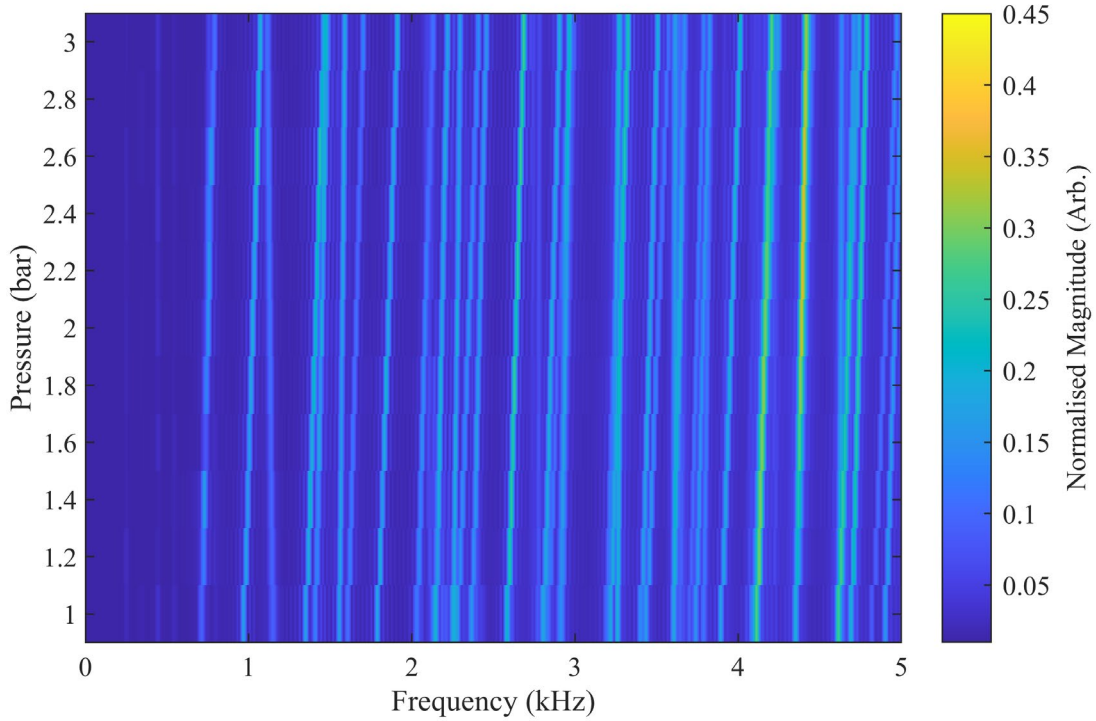

Figure 5: Image plot of the spectral response of the Magnox package wall when the detection EMAT is used to record the out-of-plane vibrations of the package wall from atmospheric pressure to 3 bar.

The vibrational resonant frequencies of the Magnox packages have been thoroughly investigated both experimentally and computationally through FE models, revealing agreement between the experimental and FE model outputs. Furthermore, the fluctuation in the vibrational frequencies of the Magnox package under increasing internal pressure has been meticulously modelled computationally and measured experimentally using the generator and detector EMATs. Both the FE model and experimental measurements affirm that as the internal pressure of the Magnox package rises, so too does the peak frequency of the vibrational frequencies. Notably, within the literature, limited research has been published concerning the measurement of internal pressure in Magnox containment packages. Therefore, the work presented in the thesis fills a significant gap in the literature and showcases a potential technique that could be implemented within the nuclear industry for the precise measurement of internal pressure in Special Nuclear Material (SNM) packages. The work presented in the thesis has resulted in the initiation of a postdoctoral research project aimed at advancing the EMAT measurement method into a prototype instrumentation device. This device will undergo trials on plant with real packages, marking a significant step forward in the practical application of the developed technique.

Elizabeth Sharp

1. **Poyry Energy Wood Nuclear.** *2019 UK Radioactive Material Inventory. .* Cumbria : Nuclear Decommissioning Authority, 2019.

2. **Nuclear Decommissioning Authority.** *Progress on Plutonium Consolidation Storage and Disposition.* Cumbria : Nuclear Decommissioning Authority, 2019.

3. **Katovsky., V. Verma and K.** *Spent nuclear fuel and accelerator-driven subcritical systems.* Singapore : Springer Nature, 2019.

4. *Maintaing Safe Storage of UK Plutonium.* **Gallagher, C. P., P. M. Cook, R. Hanratty, and M. Moorcroft.** Manchester : The Nuclear Institute , 2013.

5. **Jensen, S. E., and Erik Nonbøl.** *Description of the Magnox types of gas cooled reactor.* Denmark : s.n., 1999.

6. *Contingency Options for the Dry Storage of Magnox Spent Fuel in the UK.* **Morris, J, Wickham, S, Richardson, P, Rhodes, C, & Newland, M.** Liverpool : Proceedings of the ASME 2009 12th International Conference on Environmental Remediation and Radioactive Waste Management, 2009.

7. **International Atomic Energy Agency.** *APPLICATION OF MULTI-CRITERIA DECISION ANALYSIS METHODS TO COMPARATIVE EVALUATION OF NUCLEAR ENERGY SYSTEM OPTIONS: FINAL REPORT OF THE INPRO COLLABORATIVE PROJECT KIND.* Vienna : International Atomic Energy Agency, 2019. 24.

8. **Allen Gunter, H.** *Stabilization, packaging, and storage of plutonium-bearing.* Washington D.C : U.S Department of Energy, 2012.

9. **Nuclear Energy Agency.** *The safety of the nuclear fuel cycle.* Paris : OECD Publishing , 2005.

10. *Shape memory Alloy Tension/Compression Device for Seismic Retrofit of Buildings.* **Speicher, Matthew, et al.** s.l. : Journal of Materials, Engineering and Performance., 2009, Vol. 18.

11. *Modeling.* **Sgambitterra, Emmanuel, Maletta, Carmine and Furgiuele, Franco.** s.l. : Journal of Intelligent Material Systems and Structures, 2016, Vol. 27.1.

12. *NiTi Belleville washers:.* **Maletta, Carmine, Filice, Luigino and Furgiele, Franco.** s.l. : Journal of Intelligent Material, Systems and Structures., 2013, Vol. 24.6.

13. *Pressure monitoring of Special Nuclear Material Containment.* **Sharp, Elizabeth, et al.** s.l. : NDT&E International, 2023, Vol. 133.